Article

Vita

Transcending stereochemical boundaries: ambidextrous cleavage of D- and L-peptide enantiomers by natural eukaryotic proteases

Mengjiao Li[1,2,3#], Kai Chen[1,2,3#], Wenyang Zhang[1,2,3], Jianyi Han[1,2,3], Mengzhun Guo[1,2,3], Xinxin Zhu[1,2,3], Jia Zheng[1,2,3], Jing Huang[*1,2,3], Tian Li[*1,2,3], Bobo Dang[*1,2,3]

Proteins have predominantly evolved in the L-form, favoring homochiral interactions with other L-proteins while avoiding their D-enantiomer counterparts. Reflecting this principle, natural proteases are known to hydrolyze L-peptides but not their mirror-image D-enantiomers. In this study, we designed and screened a combinatorial D-peptide library tailored for proteases and unexpectedly revealed that several eukaryotic proteases — including papain, human cathepsin B, and mouse carboxylesterase 1c — efficiently cleave D-peptide substrates through sequence-specific recognition. The corresponding enantiomeric L-peptide substrates were also cleaved, indicating ambidextrous substrate proteolysis. Structural analyses show that cathepsin B achieves activity through enantiomer-specific substrate-binding modes, underscoring its ability to accommodate alternative stereochemistries for substrate recognition and processing. Leveraging this activity, we developed a D-peptide substrate of cathepsin B as an efficient cleavable linker for antibody–drug conjugates, demonstrating potent antitumor efficacy *in vitro* and *in vivo*. These results reveal an unanticipated capacity for substrate recognition in natural eukaryotic proteases, broadening the framework of protease specificity and enabling new possibilities for therapeutic design.

https://doi.org/10.15302/vita.2026.03.0022

INTRODUCTION

Proteins in living organisms are composed almost exclusively of L-amino acids[1,2]. Molecular interactions between natural proteins generally rely on homochiral recognition, whereby L-proteins selectively engage other L-proteins, while heterochiral interactions with their mirror-image D-counterparts are precluded by stereochemical constraints (Fig. 1a). Accordingly, inverting the chirality of one binding partner often disrupts binding, whereas simultaneous inversion of both partners can re-establish recognition via the corresponding mirror-image pair (Fig. 1a)[3–5]. Proteases follow the same general expectation: natural proteases are usually reported to hydrolyze L-peptide substrates, but not their mirror-image D-counterparts (Fig. 1b)[6]. Consequently, ambidextrous recognition — where a natural L-protein, such as a protease, selectively binds and processes both D- and L-enantiomers of a peptide substrate — is exceptionally rare, particularly in eukaryotic systems where D-amino acids are seldom used and evolutionary pressure for such interactions is minimal (Fig. 1).

For eukaryotic proteases, studies show that cathepsins B, L, and K can tolerate single D-amino acid substitutions at P3 or P4 within L-peptide substrates, whereas substitutions at P1 or P2 disrupt recognition and cleavage — consistent with fully D-peptide substrates not being hydrolyzed by these enzymes[7–9]. Moreover, it has been reported that a wide range of eukaryotic proteases are unable to hydrolyze D-peptide substrates altogether[6]. This suggests that heterochiral proteolysis may be exceedingly rare in higher organisms (Fig. 1b). The absence of proteolysis toward D-peptides and D-proteins has provided a rationale for their development as therapeutic modalities, owing to their inherent metabolic stability and low immunogenicity[4,10–15]. At the same time, this property has contributed to the concerns about potential biohazards associated with mirror-image bacteria, which may fail to trigger effective immune responses in humans and thus pose a risk of uncontrolled propagation[16].

Although eukaryotic proteases have likely experienced little direct selection for heterochiral proteolysis — perhaps contributing to its apparent rarity — they have also faced limited pressure to eliminate interactions with D-proteins or D-peptides. It is therefore plausible that heterochiral substrate recognition and catalysis could persist or re-emerge from ancestral scaffolds, even though such capacities have yet to be empirically demonstrated.

In this study, we investigated whether eukaryotic proteases possess an unrecognized capacity to cleave D-peptides, despite previous studies indicating that such enzymes are unable to hydrolyze D-peptides, thereby motivating a re-examination of the stereochemical constraints that govern protease catalysis. To this end, we constructed a synthetic combinatorial D-peptide library tailored for proteases and systematically evaluated a diverse panel of eukaryotic enzymes — including papain, proteinase K, cathepsins B, H, L, and Z, carboxylesterases 1 and 2, pepsin, and trypsin (Fig. 2a). Our results

1. Research Center for Industries of the Future and Key Laboratory of Structural Biology of Zhejiang Province, School of Life Sciences, Westlake University, Hangzhou, Zhejiang, China 2. Westlake Laboratory of Life Sciences and Biomedicine, Hangzhou, Zhejiang, China 3. Institute of Biology, Westlake Institute for Advanced Study, Hangzhou, Zhejiang, China #These authors contributed equally. *Correspondence: Jing Huang (huangjing@westlake.edu.cn), Tian Li (litian32@westlake.edu.cn), Bobo Dang (dangbobo@westlake.edu.cn)

Received: November 25, 2025; Accepted: March 27, 2026; Published: April 20, 2026

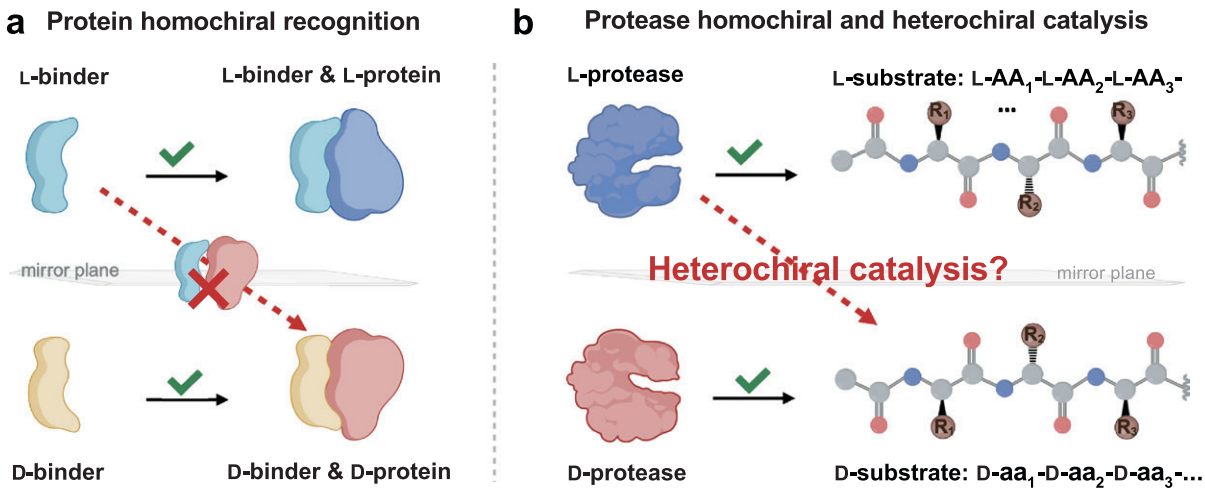

Fig. 1 The homochiral and heterochiral recognition of proteins. a The homochiral recognition principle of proteins. L-proteins bind to other L-protein binders (homochiral), while avoiding binding to the D-form of the same protein binder (heterochiral). **b** Natural proteases are characterized by L-peptide substrate-specific activity. Whether they also possess the capacity for heterochiral recognition and catalysis — processing both L- and D-peptides of the identical sequence (ambidextrous) — remains an open question.

unexpectedly revealed that papain, human cathepsin B (hCATB), and mouse carboxylesterase 1c (mCES1c) efficiently hydrolyze D-peptide substrates through sequence-specific recognition. All three proteases also cleaved the corresponding L-peptides, demonstrating ambidextrous substrate recognition and catalysis. Notably, these proteases achieve catalytic efficiencies on D-peptide substrates that rival or exceed those of benchmark proteases such as Tobacco Etch Virus (TEV) protease and Human Rhinovirus 3C (HRV3C) protease on their optimal L-peptide substrates. The D-peptide substrate of hCATB was further developed as a new cleavable linker for antibody drug conjugates (ADCs), indicating its practical application potential.

RESULTS

Papain and hCATB hydrolyze D-peptide substrates with high catalytic efficiency and sequence specificity

Although previous studies have shown that single D-amino acids can sometimes be tolerated within L-peptide substrates, fully D-peptide substrates composed of D-amino acids and the achiral glycine have generally exhibited little proteolysis by these enzymes. Here, we specifically investigated whether natural eukaryotic proteases possess the capacity to cleave mirror-image D-peptides[7–9]. Proteases typically recognize peptide substrates within a stretch of four to six amino acids, with one or two key amino acids serving as the critical recognition residues[17–19]. We constructed a combinatorial D-tetrapeptide library consisting of D-amino acids and the achiral glycine, systematically varying a single amino acid (Library #1) or a combination of two amino acids (Library #2) at different positions (Fig. 2b; Supplementary Fig. S1a and Tables S1, S2, S5, and S17). We incubated each selected protease, including papain, proteinase K, human cathepsins B, H, L, and Z, human carboxylesterases 1 and 2, pepsin, and trypsin, individually with our D-peptide libraries under their respective optimal working conditions, and assessed proteolytic activity by liquid chromatography-mass spectrometry (LC-MS) analysis (Fig. 2a). Preliminary results showed that papain exhibited promising activity (> 5% cleavage yield) against peptides from the −GGxG/a− and −GxG/Ga− libraries, where x represents D-Trp, D-Phe, or D-Tyr (slash indicates the cleavage site; Supplementary Data S1 and Tables S2–S4). hCATB was also found to cleave peptides in the −GGjGG− library, where j corresponds to D-Trp or D-Tyr (Supplementary Fig. S1b and Tables S18 and S19). More pronounced proteolytic activity of papain was observed with the two-amino-acid combinatorial libraries, particularly with −G/zzG/a−, −GzG/za−, and −zG/zG/a− (where z primarily prefers D-Leu and D-Tyr) (Supplementary Data S2 and Tables S5 and S6). Similarly, hCATB efficiently cleaved sequences including −GyyG/G−, −GyfG/G−, and −GfwG/G− (Supplementary Fig. S1c and Tables S18 and S19), indicating a preference for D-Tyr, D-Phe, and D-Trp at the P2 position, with Gly at the P1 position.

We then synthesized the identified D-peptides and confirmed their susceptibility to proteolysis. Papain cleaved 24% of peptide −yGyG/a− after 6 hours (Fig. 2c; Supplementary Tables S7 and S8), while hCATB could cleave 20% of −GGyG/G− after 12 hours (Fig. 2d; Supplementary Table S20). These results indicate that papain and hCATB possess an inherent, albeit moderate, capacity to hydrolyze D-peptide substrates. Many natural proteases recognize optimal peptide substrates, where the amino acid residues at each position contribute synergistically to the overall catalytic efficiency, as seen with TEV protease, HRV3C protease, or factor Xa[20,21]. To investigate whether D-amino acids within D-peptide substrates exhibit similar cooperative effects, we first conducted single-point mutation scans to assess the positional preference of individual D-amino acids based on the initial identified optimal substrate sequence (Fig. 2e, i). For the D-peptide substrate of papain, the P1 position only tolerated glycine (Fig. 2e). The P2 position showed a strong preference for D-Trp, while the P3 preferred glycine but also accommodated D-Ser and D-Ala. The P4 position exhibited a clear preference for aromatic residues, including D-Trp, D-Phe, and D-Tyr. In contrast, P5 showed less specificity, with D-Leu yielding the highest cleavage efficiency. The P1′ position favored hydrophobic D-amino acids, with D-Tyr being the most optimal (Fig. 2e; Supplementary Fig. S2a and Tables S8–S13).

To investigate potential cooperative effects in the D-peptide substrates of papain, we combined preferred D-amino acids at various positions and evaluated the resulting sequences. The peptide −lyGwG/y− showed a markedly accelerated cleavage rate, reaching 53% yield within 1 hour (Supplementary

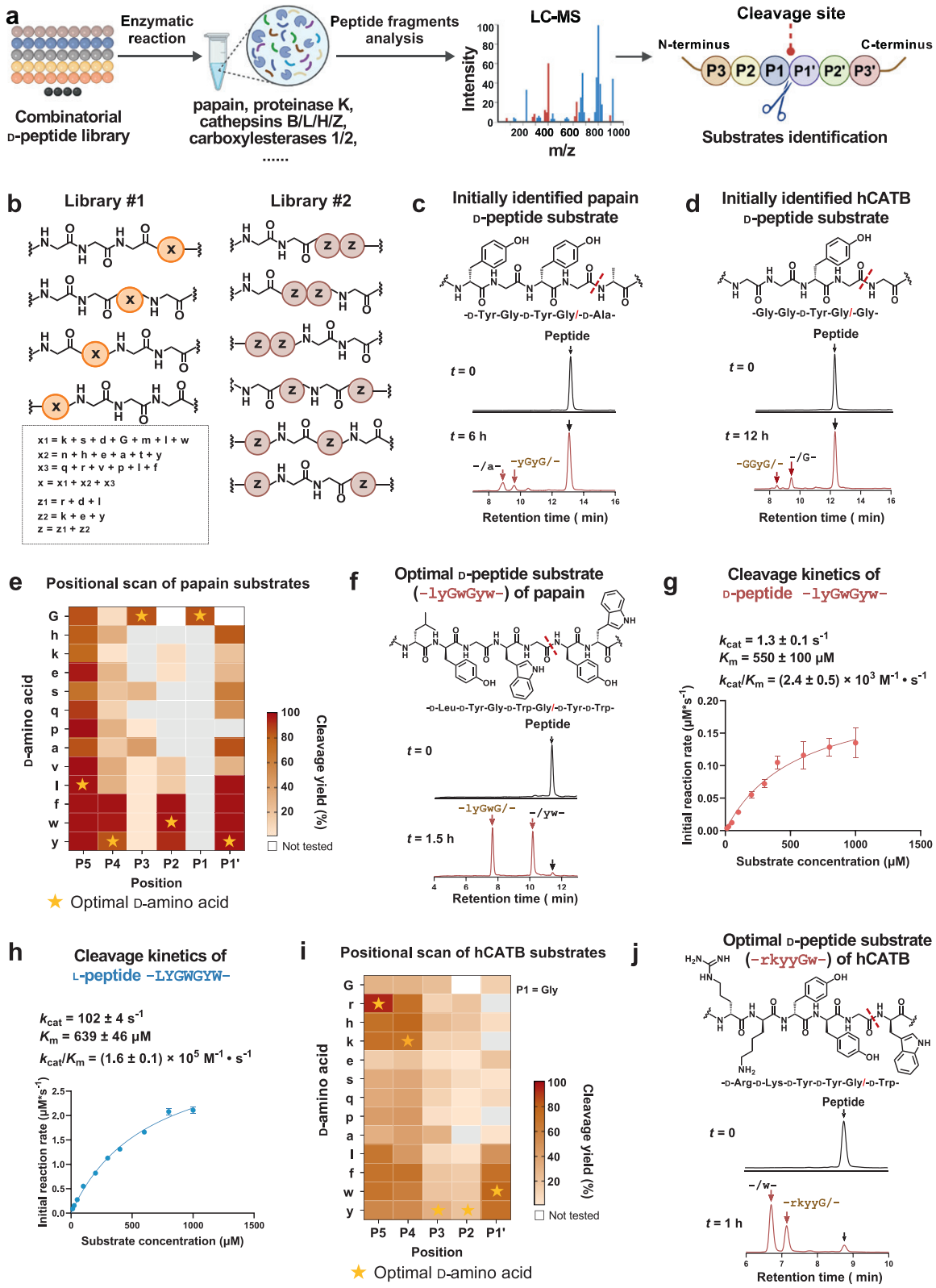

Fig. 2 Papain and hCATB hydrolyze D-peptide substrates with high specificity and efficiency. a The workflow for D-peptide substrates screening toward natural eukaryotic proteases. Substrate positions are designated according to canonical protease substrate nomenclature. **b** The design of the combinatorial D-tetrapeptide library. x and z denote different combinations of mixed amino acids, and lowercase letters represent D-amino acids. **c** Peptide −yGyGa− was the initially identified papain substrate, achieving 24% cleavage after 6 hours. The red dotted line represents the scissile bond. The black arrow in the HPLC trace indicates the intact peptide, and the colored arrows indicate the cleaved fragments. **d** Peptide −GGyGG− was the initial identified hCATB substrate, achieving 20% cleavage after 12 hours. **e** Site saturation mutagenesis screening of D-amino acids from P5 to P1′ positions based on the peptide −yGwGa− to identify optimal D-peptide substrate of papain. The stars represent optimal D-amino acids. **f** Peptide −lyGwGyw− is the optimal D-peptide substrate for papain, achieving quantitative cleavage within 1.5 hours. **g** The kinetics of papain (172 nM) cleavage of the optimal D-peptide −lyGwGyw− ($n = 3$ independent replicates, mean ± SD). **h** The kinetics of papain (34.5 nM) cleavage of the corresponding L-peptide counterpart −LYGWGYW− ($n = 3$ independent replicates, mean ± SD). **i** Site saturation mutagenesis screening of D-amino acids from P5 to P1′ positions based on the peptide −GGyGG− to identify the optimal D-peptide substrate of hCATB. **j** Peptide −rkyyGw− is the optimal D-peptide substrate for hCATB, achieving 80% cleavage within 1 hour. **c**, **e**, **f** The concentration of papain was 235 nM, and the substrate concentration was 40 μM. **i**, **j** The concentration of hCATB was 20 nM, and the substrate concentration was 40 μM.

Table S14). Further analysis of the P6 and P2′ positions revealed P2′ displaying a slight preference for hydrophobic residues, while P6 did not show strong residue preference (Supplementary Fig. S2b and Tables S15 and S16). Ultimately, considering substrate length and specificity, −lyGwG/yw− was identified as the optimal D-peptide substrate, achieving over 95% cleavage after 1.5 hours at 37 °C (Fig. 2f). We measured the kinetic constants of papain cleavage of the D-peptide −lyGwG/yw− and found a k_{cat} of 1.3 ± 0.1 s^{-1} and a K_m of 550 ± 100 μM, resulting in a k_{cat}/K_m of (2.4 ± 0.5) × 10^3 M^{-1} s^{-1} (Fig. 2g). Additionally, we evaluated the proteolytic activity of papain on the corresponding L-peptide substrate (−LYGWGYW−) (the capital letter in the sequence indicates L-amino acids) and found that the L-peptide substrate was also efficiently cleaved with a k_{cat}/K_m of (1.6 ± 0.1) × 10^5 M^{-1} s^{-1} (Fig. 2h; Supplementary Fig. S2c).

A similar investigation was conducted on the D-peptide substrate of hCATB, revealing that the P2–P4 positions exhibited varying preferences for aromatic and positively charged residues (Fig. 2i). P5 favored hydrophobic and positively charged residues, with a particularly high preference for D-Arg. Consistent with its role as a recognition site of hCATB, P1′ displayed marked specificity for aromatic amino acids (Fig. 2i; Supplementary Tables S20–S23). Combining the preferred residues at each position again revealed cooperative effects, with the optimal sequence −rkyyG/w− achieving 80% hCATB cleavage within 1 hour (Fig. 2j; Supplementary Table S24). Similarly, hCATB can also recognize and cleave the corresponding L-peptide substrate (−RKYYGW−; Supplementary Fig. S3a).

Together, these findings establish that papain and hCATB possess ambidextrous substrate cleavage capabilities, recognizing both D- and L-peptide enantiomers and efficiently cleaving the optimal D-peptide sequence identified by combining preferred D-amino acids at specific substrate positions.

Structural analysis of hCATB recognition of D- and L-peptide substrates

To gain deeper insight into hCATB's interaction with its D-peptide substrate, we synthesized Ac−rkyyG−Cl (Supplementary Fig. S3b and Data S3a) as a hCATB covalent inhibitor to target its catalytic Cys29 for structural characterizations[22,23]. Ac−rkyyG−Cl successfully formed a covalent bond with hCATB (Supplementary Data S4 and Fig. S3b, c), enabling crystallization of the complex and structure determination at an average resolution of 1.5 Å (PDB: 9XHR; Supplementary Table S25). The D-peptide forms a stable complex within the active site of hCATB, with a covalent bond to the catalytic residue Cys29 clearly resolved (Fig. 3a–d). There were six hydrogen bonds between the D-peptide substrate and the protease: P1-Gly with Gln23 and Cys29, P2-D-Tyr with Gly74 and Glu245, and P4-D-Lys with Ser175 and Gly198 (Fig. 3c). The side chain of P2-D-Tyr was well-positioned in the active pocket, while the P3-D-Tyr side chain extended outward, and the P5-D-Arg and P3-D-Tyr side chains were not well resolved in the electron density map (Fig. 3b–d).

To compare the recognition modes of hCATB toward the D-peptide and its enantiomeric L-peptide counterparts, we also prepared the L-peptide-based covalent inhibitor Ac−RKYYG−Cl and a truncated L-peptide substrate, Ac−YYG−Cl (Supplementary Data S3b–d). Only the co-crystal structure of hCATB in complex with Ac−YYG−Cl was successfully obtained (PDB: 9VA8; Supplementary Table S26), revealing a well-resolved electron density map for the bound peptide (Fig. 3a–d). The structure revealed that the L-peptide substrate (−YYG−) interacts with hCATB in a different manner, binding at the opposite side of the binding groove compared to the D-peptide substrate, forming four hydrogen bonds with hCATB: P1-Gly with Gln23 and Cys29, and P2-D-Tyr with Gly121 and Trp221 (Fig. 3a–c). Interestingly, the loop Thr120–Gly123 of hCATB went through a conformational change to accommodate the binding of the L-peptide substrate (Supplementary Fig. S3d). In addition, we validated that the truncated L-peptide −YYG− substrate was also cleaved by hCATB, exhibiting comparable catalytic efficiency to the D-peptide substrate −rkyyG− (Supplementary Fig. S3e). For a more rigorous comparison between the L- and D-enantiomers, we crystallized hCATB modified with Ac−yyG−Cl. Unfortunately, unlike the Ac−rkyyG−hCATB and Ac−YYG−hCATB complexes, the local electron density corresponding to Ac-yyG in the hCATB structure was poorly resolved (Supplementary Fig. S4), indicating the presence of multiple interacting conformations of this substrate.

The D-peptide substrate of hCATB was developed as a cleavable linker for ADCs

Cathepsin B is implicated in various physiological and pathological processes[24,25]. For instance, Cathepsin B is overexpressed in many tumors, and its peptide substrates have been used to design cleavable linkers for payload release in ADCs[24,26]. Currently, the most commonly used enzyme-cleavable linkers are based on short peptides, such as −Gly-Gly-Phe-Gly−(−GGFG−) and −Val-Cit−(−VC−), which are found in commercial ADCs[27]. The ability of −rkyyG− to be efficiently cleaved by cathepsin B suggests its potential for designing new ADCs. Moreover, many current peptide linkers used in ADCs are hydrophobic, which can contribute to their instability. In contrast, −rkyyG− contains two positively charged residues, significantly enhancing the hydrophilicity of the linker. Additionally, the D-peptide configuration ensures greater stability in plasma, contributing to the overall stability of the designed ADCs.

We introduced a spacer, 3-(4-aminophenyl) propionic acid, at the C-terminus of the D-peptide substrates to mimic the self-immolative p-aminobenzyl carbamate (PAB) spacer commonly used in ADCs (Supplementary Fig. S3f). This modification proved fully compatible with the −rkyyG− sequence, resulting in complete cleavage within 30 minutes (Supplementary Fig. S3e and Table S27). We measured the cleavage kinetic parameters of hCATB on the −rkyyG/spacer− substrate and found a k_{cat} of 30 ± 3 s^{-1} and a K_m of 649 ± 111 μM, resulting in a k_{cat}/K_m of (4.6 ± 0.6) × 10^4 M^{-1} s^{-1} (Fig. 3e). In comparison, the kinetic parameters of hCATB on the commercial ADC linkers −VC− and −GGFG− yielded k_{cat}/K_m values of (9.7 ± 1.9) × 10^4 M^{-1} s^{-1} and (3.4 ± 0.4) × 10^3 M^{-1} s^{-1}, respectively (Fig. 3f, g). Thus, the D-peptide linker demonstrates enzymatic efficiency comparable to these widely used L-peptide ADC linkers, positioning it as a strong candidate for efficient drug release in ADCs. Then pH-dependent activity was evaluated, and −rkyyG/spacer− was found to be optimally cleaved at pH 5.5–6.0 (Supplementary Fig. S5), consistent with endosomal and lysosomal conditions where ADC payloads are expected to be released. Furthermore, the observed k_{cat}/K_m

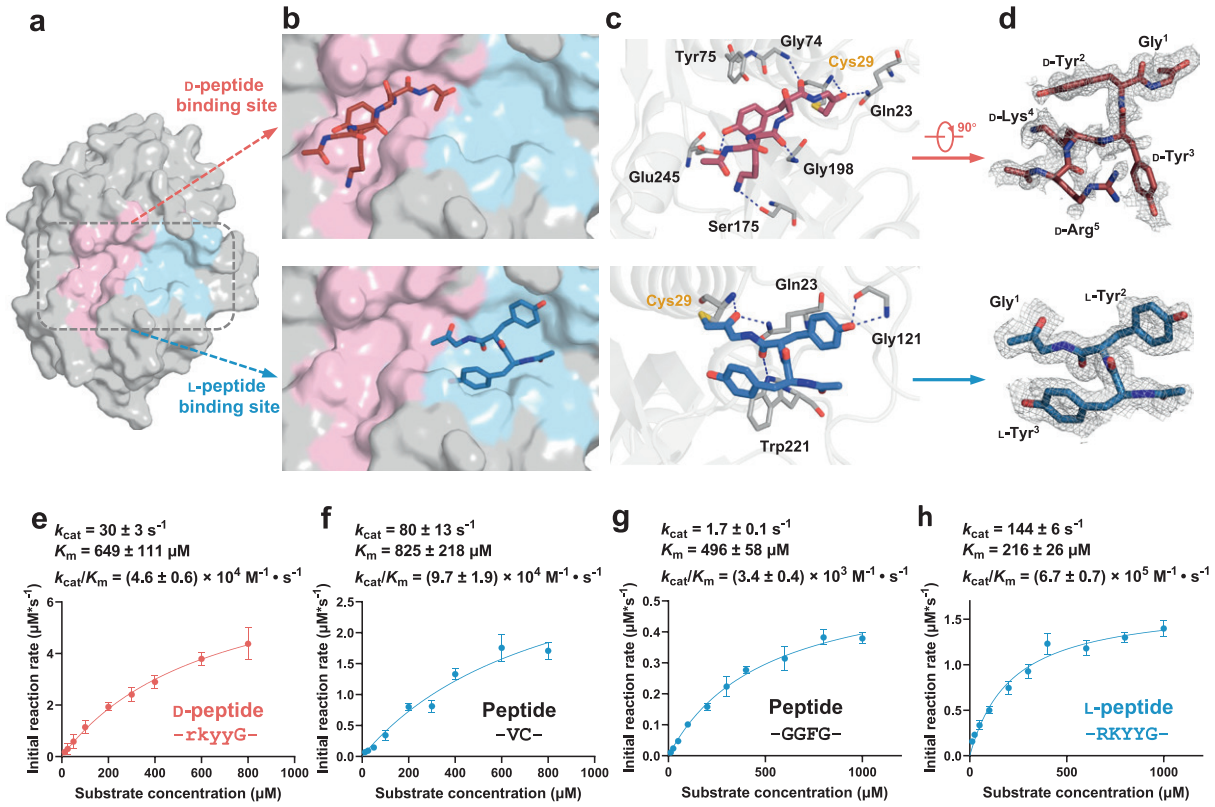

Fig. 3 Crystal structures of hCATB bound to D- and L-peptide substrates, and hCATB cleavage kinetics of different peptide substrates. **a** Surface representation of hCATB showing the D-peptide substrate binding site (pink) and the L-peptide substrate binding site (light blue), highlighting their distinct spatial locations. **b** Structural comparison of D-peptide (−rkyyG−, upper panel, dark red) and L-peptide (−YYG−, lower panel, dark blue) binding within the catalytic pocket of hCATB. **c** Hydrogen bonding interactions (blue dotted lines) between hCATB (gray) and the D-substrate (upper panel, dark red) or L-substrate (lower panel, dark blue), with interacting residues shown as sticks. Both substrates are covalently linked to the catalytic residue Cys29. **d** The Fo-Fc omit maps of D-peptide substrate (upper panel, dark red) and L-peptide substrate (lower panel, dark blue) are displayed separately as a gray mesh at a contour level of 1.0 σ. **e** hCATB (258 nM) cleavage kinetics of the optimal D-peptide −rkyyG− ($n = 4$ independent replicates, mean ± SD). **f** hCATB (47 nM) cleavage kinetics of the commercial ADC linker peptide −VC− ($n = 3$ independent replicates, mean ± SD). **g** hCATB (349 nM) cleavage kinetics of the commercial ADC linker peptide −GGFG− ($n = 3$ independent replicates, mean ± SD). **h** hCATB (7 nM) cleavage kinetics of the L-peptide counterpart −RKYYG− ($n = 3$ independent replicates, mean ± SD).

value of hCATB acting on the D-peptide linker is comparable to those of the widely used proteases. For example, TEV protease has a k_{cat}/K_m value of 7.0×10^3 M^{-1} s^{-1}, HRV3C protease has a k_{cat}/K_m value of 6.1×10^3 M^{-1} s^{-1}[20], and Factor Xa has a k_{cat}/K_m value of 3.0×10^4 M^{-1} s^{-1} for its optimal peptide substrate[21]. These findings show that hCATB possesses the capability to proteolyze D-peptide substrates with an efficiency rivaling or exceeding those of widely used natural L-proteases, underscoring its effective heterochiral catalytic function. In addition, we measured the catalytic efficiency of hCATB toward the corresponding L-peptide substrate −RKYYG−, which showed a k_{cat}/K_m value of $(6.7 \pm 0.7) \times 10^5$ M^{-1} s^{-1} (Fig. 3h), indicating ambidextrous substrate recognition and catalysis.

Next, we attached −rkyyG−PAB-MMAE to the anti-HER2 antibody trastuzumab (Tz) to prepare a homogeneous ADC (Fig. 4a). Additionally, we created a positive control ADC using the commercially used −VC−PAB-MMAE, following the same procedure. Cytotoxicity assays confirmed that the ADC constructed with our D-peptide linker could effectively kill HER2-positive SK-BR-3 cells ($HER2^{++}$, $IC_{50} = 0.044 \pm 0.005$ nM) and JIMT-1 cells ($HER2^{++}$, $IC_{50} = 0.032 \pm 0.002$ nM) while exhibiting minimal toxicity to HER2-negative MCF-7 cells (Fig. 4b). The positive control ADC (with −VC−PAB-MMAE) showed expected cytotoxic activity towards HER2-positive cells. Additionally, none of the ADCs exhibited cytotoxicity to CHO-K1 cells, indicating the prepared ADC activities are target-dependent (Fig. 4b).

We assessed the stability of the D-peptide linker ADC (Tz−rkyyG−MMAE) in human, Sprague-Dawley rat, and mouse plasma, comparing it to an ADC constructed with the commonly used −VC− linker. The results showed that Tz−rkyyG−MMAE remained stable across all three plasmas, retaining more than 73%, 85%, and 67% of intact ADC after 14 days of incubation (Fig. 4c; Supplementary Table S28). In comparison, Tz−VC−MMAE showed reasonable stability in human and Sprague-Dawley rat plasma, retaining over 55% and 68% of the intact ADC after 14 days. However, it was highly unstable in mouse plasma, with less than 20% remaining after 10 minutes (Fig. 4c; Supplementary Table S28), likely due to rapid cleavage by mCES1c targeting the −VC− linker[28,29]. *In vivo* stability tests in mice further confirmed that Tz−rkyyG−MMAE exhibited significantly better stability than Tz−VC−MMAE (Fig. 4d; Supplementary Table S29).

To evaluate the broad compatibility of the D-peptide as a cleavable linker for different ADCs, we prepared an anti-CLDN18.2 ADC using −rkyyG−PAB-MMAE, along with a positive control using −VC−PAB-MMAE. Testing on AsPC-1-CLDN18.2 pancreatic cancer cells and NUGC-4 gastric cancer cells ($CLDN18.2^{+}$) revealed that the D-peptide linker ADC exhibited comparable cytotoxic activity to control, with IC_{50} values of 2.5 ± 1.2 nM for AsPC-1-CLDN18.2 and 0.5 ± 0.1 nM for

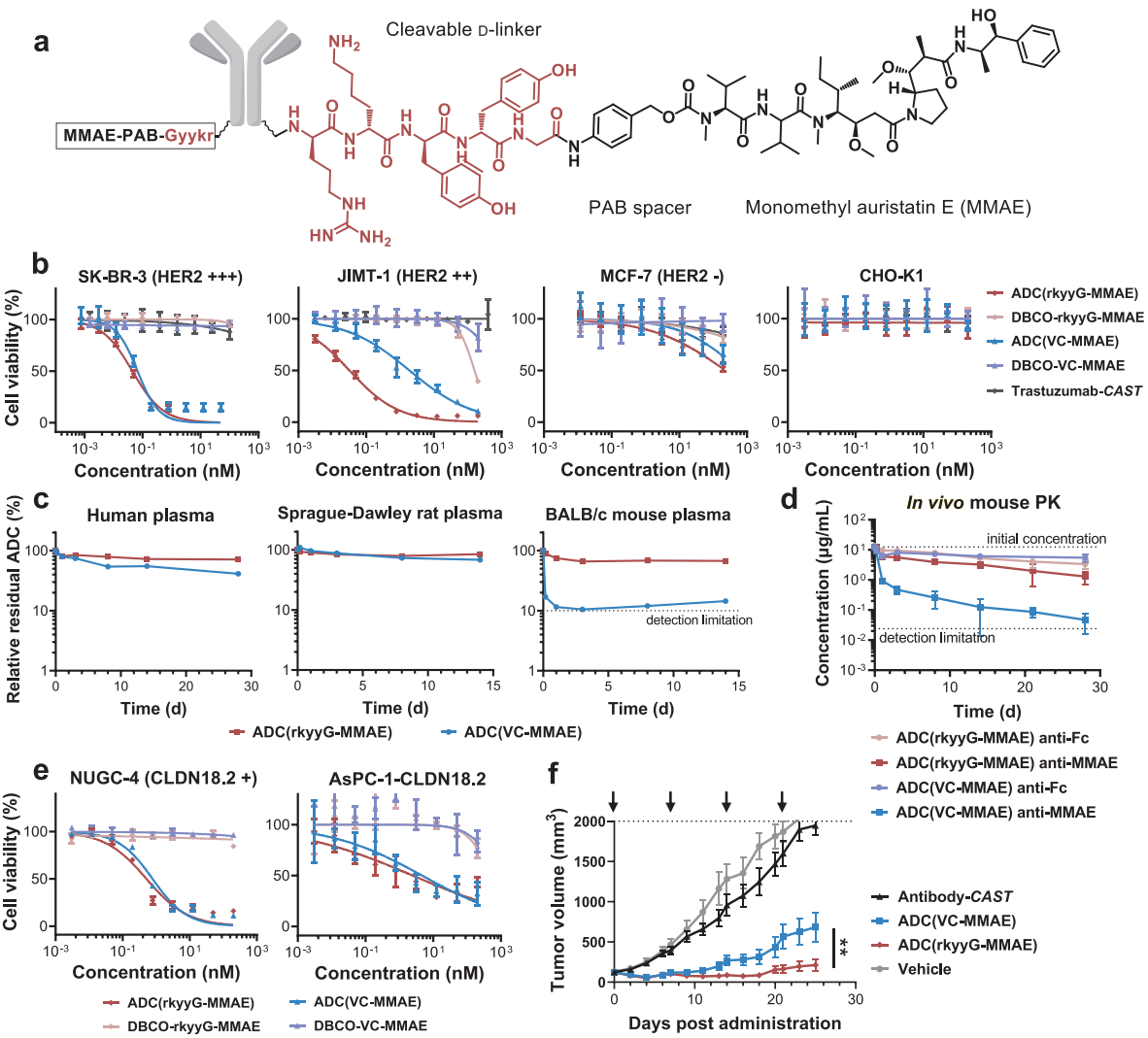

Fig. 4 The D-peptide substrate of hCATB was developed as a cleavable linker for ADCs. a Chemical structure of ADC constructed using D-peptide −rkyyG−. **b** Cytotoxicity of anti-HER2 ADCs in tumor cells. ADC(rkyyG-MMAE): SK-BR-3 (IC_{50} = 0.044 ± 0.005 nM), JIMT-1 (IC_{50} = 0.032 ± 0.002 nM), and MCF-7 (IC_{50} = 229 nM ± 59 nM). ADC(VC-MMAE): SK-BR-3 (IC_{50} = 0.067 ± 0.010 nM), JIMT-1 (IC_{50} = 1.9 ± 0.2 nM), and MCF-7 (IC_{50} = 610 nM ± 550 nM) (*n* = 3 independent replicates, mean ± SD). **c** *In vitro* plasma stability of anti-HER2 ADCs across different species (*n* = 3 independent replicates; mean values of concentrations were analyzed). **d** *In vivo* pharmacokinetics of anti-HER2 ADCs in mice following tail vein injection at 1 mg/kg (*n* = 6). **e** Cytotoxicity of anti-Claudin 18.2 ADCs in tumor cells. ADC(rkyyG−MMAE): AsPC-1-CLDN18.2 (IC_{50} = 2.5 ± 1.2 nM) and NUGC-4 (IC_{50} = 0.5 ± 0.1 nM). ADC(VC−MMAE): AsPC-1-CLDN18.2 (IC_{50} = 4.7 ± 2.1 nM) and NUGC-4 (IC_{50} = 0.8 ± 0.1 nM). (*n* = 3 independent replicates, mean ± SD). **f** *In vivo* tumor suppression efficacy of ADCs in the NUGC-4 xenograft model. Data points represent mean values, with error bars indicating SEM (*n* = 6). Statistical analysis was performed in GraphPad Prism 9.5 using an unpaired two-tailed *t*-test comparing ADC(rkyyG−MMAE) and ADC(VC−MMAE), yielding *P* = 0.0061.

NUGC-4 (Fig. 4e). Additionally, neither ADC showed cytotoxic effects on CHO-K1 cells, confirming the specificity of the ADCs (Supplementary Fig. S6).

We further evaluated the *in vivo* efficacy of anti-CLDN18.2 ADCs constructed with the D-peptide linker, comparing them to ADCs using the commercial −VC− linker in NUGC-4 xenograft tumor models (Fig. 4f; Supplementary Fig. S7). Both ADCs demonstrated potent antitumor activity, significantly suppressing tumor growth (Fig. 4f). Notably, following the second dose, the D-peptide linker ADC began to exhibit superior efficacy, a trend that persisted through the end of the study. This enhanced performance is likely attributable to the higher plasma stability of the D-peptide linker, which may have enabled more efficient drug delivery to the tumor site.

The cathepsin family comprises a range of proteases, among which cathepsins B, L, and S have been implicated in the cleavage of ADC linkers[30]. To assess the specificity of the D-peptide linker, we examined whether it was selectively recognized by cathepsin B or could also be cleaved by other cathepsins, including hCATA, hCATC, hCATL, hCATS, and hCATV. Our results showed that the −rkyyG/spacer− exhibited high selectivity for hCATB, achieving 100% cleavage after 30 minutes (Supplementary Fig. S3e), while none of the other cathepsins could cleave the D-peptide substrate visibly, even when using more than 10 times the amount of proteases and extending the incubation time to 12 hours (Supplementary Fig. S8 and Table S30). In contrast, most cathepsins efficiently cleaved the −VC/spacer− and −GGFG/spacer− linkers (Supplementary Fig. S8 and Table S30). The high specificity of −rkyyG/spacer− for hCATB suggests potential safety advantages in ADC applications by minimizing unintended premature payload release and associated toxicity.

Together, these data suggest that the D-peptide linker identified for hCATB can be efficiently cleaved and may be well-suited for various ADC applications, potentially offering improved hydrophilicity, enhanced stability, and greater selectivity compared to existing linker designs.

mCES1c hydrolyzes glycine-free, all D-peptide substrates with high catalytic efficiency and sequence specificity

During the plasma stability study of ADC (Tz−rkyyG−MMAE), we still observed some degradation in mouse plasma, despite the expectation that D-peptides should be completely stable. Previous studies have shown that mCES1c is responsible for the instability of the −VC− linker, leading us to hypothesize that mCES1c might also show some level of activity on the −rkyyG− peptide. Upon incubation with mCES1c, we observed low catalytic activity, with approximately 20% of the −rkyyG/− peptide cleaved after 24 hours (Fig. 5a).

We next examined whether the D-peptide substrate could be further optimized for mCES1c. Single-site mutagenesis revealed a strong P1 preference for D-Trp, D-Phe, or D-Tyr, a P2 preference for D-Leu, high P3 selectivity for hydrophobic residues, especially D-Trp, and a P4 preference for D-Leu (Fig. 5b; Supplementary Data S5 and Tables S31–S34). By combining the preferred D-amino acids at each position, we again observed a synergistic effect and identified the sequence −rlwlw/−, which achieved over 90% cleavage within 1 hour at 37 °C (Fig. 5c). Kinetics analysis showed that mCES1c proteolyzed the D-peptide −rlwlw/− with a k_{cat} of 2.3 ± 0.2 s^{-1} and a K_m of 398 ± 67 μM, yielding a catalytic efficiency (k_{cat}/K_m) of (5.7 ± 0.6) × 10^3 M^{-1} s^{-1} (Fig. 5d). mCES1c was also found to proteolyze the corresponding L-peptide substrate −RLWLW−. However, in contrast to the papain and hCATB cases, the L-peptide substrate −RLWLW− was cleaved by mCES1c with lower catalytic efficiency, exhibiting a k_{cat}/K_m of (1.6 ± 0.2) × 10^3 M^{-1} s^{-1} (Fig. 5e; Supplementary Fig. S9).

These findings suggest that eukaryotic proteases could also recognize and efficiently cleave all glycine-free D-peptides. In certain cases, D-peptides may be recognized and processed more efficiently than their L-peptide counterparts, even though L-proteases predominantly prefer L-peptide substrates.

Molecular dynamics (MD) study of enantiomeric substrate recognition by different proteases

We next performed MD simulations to gain mechanistic insight into the recognition of enantiomeric substrates by hCATB, papain, and mCES1C. We first validated the simulation setup using hCATB complex structures with Ac−rkyyG−Cl or Ac−YYG−Cl. In both cases, the substrates remained stably bound to hCATB throughout the simulations (Supplementary Fig. S10 and Videos S1, S2). We then examined the recognition of the D-tripeptide (−yyG−) by hCATB, starting from the experimentally resolved Ac−rkyyG−Cl–hCATB complex and computationally removing the two N-terminal residues. In contrast to the stable binding observed for the L-tripeptide (−YYG−), the D-tripeptide (−yyG−) displayed pronounced conformational heterogeneity during the simulations, consistent with the inability to assign a single well-defined conformation in the crystal structure (Supplementary Fig. S10 and Videos S2, S3).

Computational modeling of substrate recognition in papain and mCES1c reveals distinct chiral recognition mechanisms. In

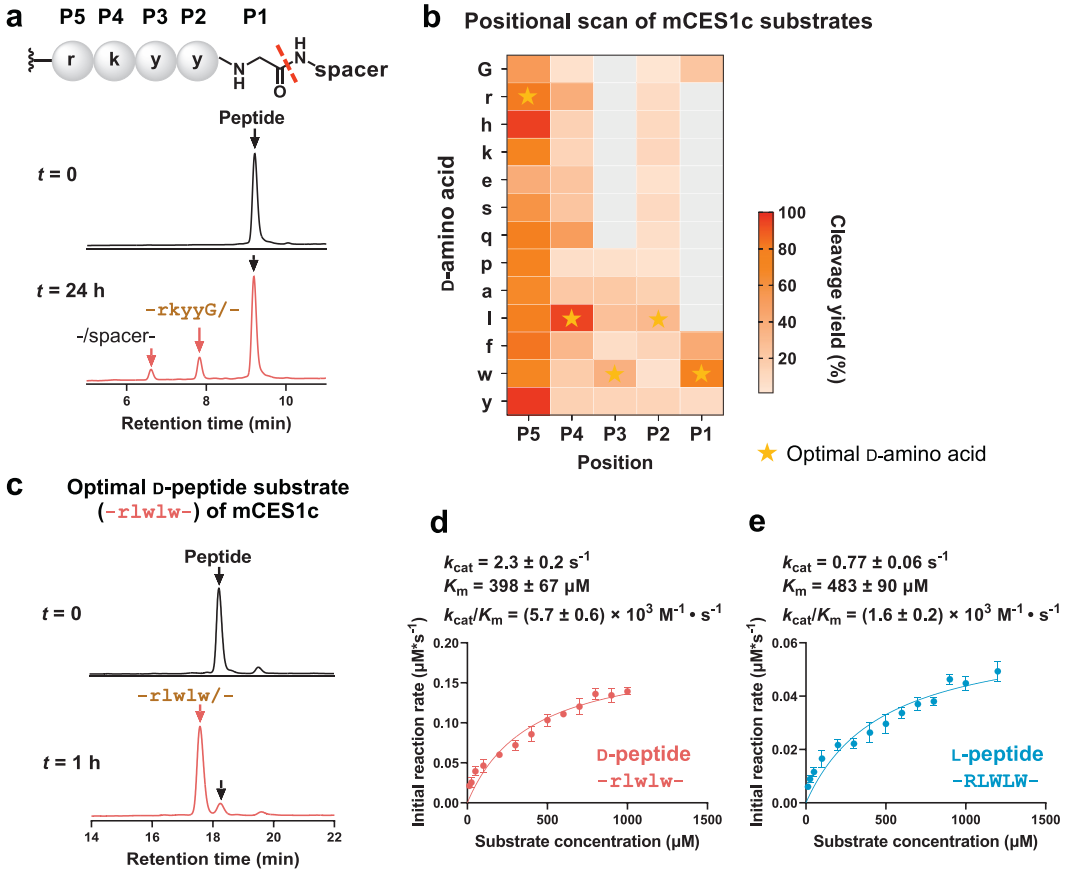

Fig. 5 mCES1c recognizes and hydrolyzes Gly-free D-peptide substrate with high specificity and efficiency. a The peptide −rkyyG-spacer− was initially identified as a substrate of mCES1c, achieving 20% cleavage after 24 hours. The red dotted line is the scissile bond. The black arrow indicates the intact peptide, while the colored arrow indicates the cleaved fragments. **b** Site saturation mutagenesis screening of D-amino acids from P5 to P1 positions to identify the optimal D-peptide substrate of mCES1c. **c** Peptide −rlwlw− is the optimal D-peptide substrate for mCES1c, achieving over 90% cleavage within 1 hour. The concentration of mCES1c was 33.7 nM, and the substrate concentration was 40 μM (**a**–**c**) . **d**, **e** The kinetics of mCES1c (84 nM) cleavage of D-peptide −rlwlw− (**d**) and the corresponding L-peptide −RLWLW− (**e**) (n = 3 independent replicates, mean ± SD).

papain, L- and D-peptides bind to the same substrate-binding pocket and engage similar interacting residues, despite adopting different conformations during the MD simulations; in both cases, π–π stacking with Tyr67 and with Trp177 contributes to enantiomeric substrate recognition (Supplementary Fig. S11 and Videos S4, S5). In contrast, mCES1c displays strong asymmetry in binding poses between chiral substrates: the L-peptide (−RLWLW−) is stabilized by a C-terminal hydrogen-bonding network, whereas the D-peptide (−rlwlw−) binds in a distinct pose characterized by a salt bridge with Glu228 (Supplementary Fig. S12 and Videos S6–S8). Together, these results indicate that chiral recognition reflects different balances between pocket plasticity and conformational flexibility and is highly system-specific.

DISCUSSION

Natural proteins are inherently homochiral, restricting interactions with partners of the same chirality and excluding D-enantiomers. Consequently, inverting the chirality of one interacting partner — such as switching from an L-peptide substrate to a D-peptide substrate — usually disrupts protease recognition and catalysis. Although it has been shown that heterochiral binding interactions can be engineered — for example, via mirror-image phage display, *de novo* design, or retro-inverso peptides — these systems enforce strict chiral complementarity: inverting the chirality of either partner abolishes binding, reflecting the absence of the reported ambidextrous recognition in this study[4,10–15]. In prokaryotic systems, certain enzymes have evolved to recognize short D-peptides (e.g. D-Ala–D-Ala) for functional purposes, yet they retain chiral fidelity and do not act on the corresponding L-substrates — indicating little capacity for ambidextrous substrate interactions[31–34]. Rare natural exceptions include GroEL/ES chaperonin folding both L- and D-DapA proteins and prothymosin-α binding peptide enantiomers[35,36]. These interactions appear to be driven primarily by nonspecific hydrophobic and electrostatic forces[35,36]. Accordingly, ambidextrous interactions with defined molecular specificity and efficient substrate catalysis, such as those mediated by proteases, have not been previously demonstrated.

Here, through combinatorial screening of D-peptide libraries, we discovered three eukaryotic proteases — papain, hCATB, and mCES1c — that had not previously encountered D-proteins evolutionarily, yet could specifically and efficiently cleave D-peptide substrates, with k_{cat}/K_m values ranging from 2.4×10^3 M^{-1} s^{-1} to 4.6×10^4 M^{-1} s^{-1}. These proteases were also found to hydrolyze the corresponding L-peptide with the same sequence, marking the discovery of ambidextrous proteolytic activity, where an L-protease can interact and efficiently cleave both the L- and D-enantiomers of the same peptide sequence.

In our study, three of the ten proteases evaluated exhibited heterochiral catalytic activity toward D-peptides. Although this activity is not generalizable across all proteases, its presence in multiple enzymes indicates that heterochiral catalysis is not an isolated exception and may be uncovered more frequently through expanded protease screening. Notably, when assayed at higher enzyme concentrations, hCATL was also found to cleave D-peptide substrates with sequence preferences similar to those of cathepsin B, albeit with substantially lower catalytic efficiency (Supplementary Fig. S13 and Tables S35 and S36). This reduced efficiency likely accounts for why such activity was not detected in the initial screens conducted at lower enzyme concentrations. The shared substrate recognition pattern between hCATB and hCATL is likely attributable to their close structural similarity (Supplementary Data S6).

The proteases capable of heterochiral recognition exhibit promiscuous substrate specificity toward L-peptides, which may confer the flexibility required to accommodate and process D-peptides. Yet, in contrast to their broad acceptance of diverse L-peptide sequences, these proteases exhibit high sequence specificity for D-peptides, efficiently cleaving only optimal D-peptide substrates at defined sites. This stringent sequence requirement likely explains why such heterochiral activity has gone unnoticed in previous studies. We speculate that other proteases with promiscuous specificity toward L-peptide substrates may likewise possess the flexibility to recognize and cleave D-peptide substrates, warranting further investigation. For such efforts, we recommend a strategy similar to the one we employed — comprehensive screening of combinatorial D-peptide libraries. Moreover, even more sophisticated library designs could be implemented, drawing on precedents established for L-peptide substrate profiling[18,37]. Such systematic investigations may uncover additional proteases capable of proteolyzing D-peptides, opening avenues for diverse downstream studies.

However, we note that L-peptide substrate promiscuity alone does not guarantee the recognition or processing of D-peptides. In our experiments, the closely related proteases hCATH and hCATZ did not cleave D-peptide substrates, nor did proteinase K, despite their reported L-peptide substrate promiscuity (Supplementary Data S6–S9). These results indicate that L-peptide promiscuity is a necessary but not sufficient condition for D-peptide catalysis, and that each protease must be individually evaluated for its ability to process D-peptide substrates. Moreover, establishing a clear relationship between protease structure and D-peptide cleavage capability remains challenging based on the current dataset. Papain and the cathepsins examined here share a similar overall structural scaffold and substrate-binding pocket architecture and conserve several active-site residues (Supplementary Data S6), yet only papain and hCATB efficiently cleave D-peptides with distinct sequence preferences, with hCATL exhibiting only marginal activity. In contrast, hCATH and hCATZ showed no detectable D-peptide cleavage. Generalization of this D-peptide cleavage phenomenon will require further investigation. For proteases with high substrate specificity, such as trypsin, cleavage of D-peptide substrates is unlikely. These enzymes possess rigid, chiral-specific binding pockets optimized for L-peptides, with substrate recognition dominated by stereospecific P1–S1 interactions. In trypsin, the S1 pocket forms specific ionic interactions with L-arginine or L-lysine at the P1 position, and the inverted chirality of D-amino acids creates an unavoidable mismatch at this interface. This mismatch cannot be compensated by other enzyme–substrate interactions, explaining why trypsin and, similarly, specific proteases fail to recognize and cleave D-peptide substrates, consistent with our experimental observations. Importantly, the observed D-peptide catalytic efficiencies (k_{cat}/K_m ranging from 2.4×10^3 M^{-1} s^{-1} to 4.6×10^4 M^{-1} s^{-1}) are comparable to those of the widely used proteases — such as TEV protease, HRV3C protease, and Factor Xa — acting on their optimal substrates (k_{cat}/K_m values: 6.0×10^3 M^{-1} s^{-1} to 3.0×10^4 M^{-1} s^{-1})[20,21]. These findings suggest that eukaryotic proteases can indeed recognize and cleave D-peptide substrates with comparable efficiencies to

those observed for natural L-peptides. In each case we examined, the individual D-amino acids at different positions of the D-peptide substrate acted cooperatively, collectively enhancing the catalytic efficiency of the optimal substrate — similar to how natural proteases such as TEV protease and HRV3C protease recognize their optimal substrates.

Given that hCATB is widely used for payload release in ADCs, we adapted its D-peptide substrate into a cleavable linker and characterized its performance. The resulting D-peptide linker exhibited high aqueous solubility, strong plasma stability, and cleavage efficiency comparable to commercial linkers such as −GGFG− and −VC−. ADCs constructed with this linker achieved potent tumor suppression in cell assays and superior efficacy in xenograft models. Importantly, while the commercial linkers are susceptible to cleavage by multiple cathepsins, the D-peptide linker was selectively cleaved by hCATB, with no obvious activity from other closely related cathepsins. This high level of protease specificity suggests that D-peptide linkers could provide more precise payload release, potentially reducing the off-target toxicity and improving the therapeutic window. Collectively, these properties highlight the promise of D-peptide linkers as a selective and robust alternative to conventional ADC linkers, warranting further exploration in targeted therapeutic development.

In summary, we designed a tailored synthetic D-peptide combinatorial library and revealed a hidden capacity of natural eukaryotic proteases to recognize and efficiently cleave both L- and D-peptides of identical sequence. This discovery extends the current understanding of protease specificity by revealing unexpected flexibility in substrate recognition and demonstrating that ambidextrous protease recognition occurs in defined contexts. These findings may further suggest a broader framework for biomolecular interactions, potentially rooted in the origins of molecular recognition or preserved through latent evolutionary processes. Given the central role of proteases across diverse physiological pathways, this discovery offers a foundation for innovative applications spanning next-generation protease inhibitors, activity-based probes, peptide-based self-assembly materials, and highly selective cleavable linkers for prodrugs — establishing new opportunities for precision therapeutics, diagnostics, and molecular engineering.

MATERIALS AND METHODS

Peptide synthesis

All screened peptides were synthesized on a 0.01 mmol scale using an automated parallel peptide synthesizer (Syro II, Biotage) at room temperature unless otherwise stated. Fmoc-Rink amide resin was utilized. Each amino acid was double coupled, and the cycle comprised 12 minutes of coupling with 200 µL of Fmoc-protected amino acid (0.5 M in *N*,*N*-dimethylformamide (DMF)), 200 µL of 1-[Bis(dimethylamino) methylen]-5-chlorobenzotriazolium 3-oxide hexafluorophosphate (HCTU) (0.475 M in DMF) and 100 µL of *N*,*N*-diisopropylethylamine (2 M in *N*-Methyl-2-pyrrolidone (NMP)), followed by a 3-minute wash with DMF three times, deprotection with 20% (v/v) 4-methyl piperidine (PIP) in DMF once, and a 3-minute wash with DMF four times. Upon completion, acetylation of the N-terminus was achieved using acetic anhydride:*N*,*N*-Diisopropylethylamine (DIEA):DMF in a 1:1:8 ratio at room temperature for 30 minutes, followed by four DMF washes. The resins were then extensively washed with dichloromethane (DCM) and dried under vacuum. Peptides were cleaved from the resins and side chains were deprotected using a cocktail of 2.5% (v/v) water and 2.5% (v/v) triisopropylsilane in neat trifluoroacetic acid for 2 hours at room temperature. The resulting peptide solution was filtered, precipitated, and washed with cold diethyl ether twice. After evaporation, the peptide solid was dissolved in 50% solvent A/B (v/v) and lyophilized. The molecular weight and purity of peptides were confirmed by LC-MS.

HPLC and LC-MS analysis

LC-MS analysis was performed using an Agilent 1260-6230 single Time of Flight (ToF) LC-MS. The column used was Agilent ZORBAX 3.5 µm 300SB-C18 and Agilent ZORBAX 5 µm 300SB-CN.

Nomenclature rules

Following the IUPAC (International Union of Pure and Applied Chemistry) and IUB (International Union of Biochemistry) nomenclature rules, common amino acids are represented by a one-letter symbol or a three-letter symbol. The D-configuration is indicated by adding "D-" before the three-letter code or by using the one-letter code with the "D-" prefix. Peptide sequences are written from the N-terminus (amino terminus) to the C-terminus (carboxyl terminus), and the "D-" prefix is used for each D-amino acid in the sequence. A hyphen separates the amino acids in the sequence. The cleavage site is typically indicated by a slash (/) between the scissile bond. The positions around the scissile bond are labeled from Pn to Pn′. Pn denotes the general term for the amino acid residue n positions N-terminal to the scissile bond, and Pn′ denotes the general term for the amino acid residue n positions C-terminal to the scissile bond. For example, -P3-P2-P1/P1′-P2′-P3′-. Additionally, any modifications to the amino acids are indicated by their respective symbols or abbreviations (Ac- for an N-terminally acetylated peptide, e.g.,).

Combinatorial D-peptide library

D-Amino acids existed in combinatorial substrate libraries: k, s, d, G, m, l, w, n, h, e, a, t, y, q, r, v, p, i, and f. These D-amino acids were mixed in different relative ratios to ensure an equal distribution in the synthesized peptides (Supplementary Table S1)[38,39]. The combinatorial substrate Library #1 encompasses all these D-amino acids (x), categorized into three groups (x_1–x_3) based on their properties (Supplementary Table S2). The combinatorial substrate Library #2 encompasses six D-amino acids (z), categorized into two groups (z_1 and z_2) based on their properties (Supplementary Table S5). The combinatorial substrate Library #1/#2 features a Gly residue at the C-terminus of the screened D-peptide and consists of 12 D-amino acids (j), categorized into three groups (j_1–j_3) based on their properties (Supplementary Table S17). The combinatorial substrate Library #3 incorporates 19 D-amino acids (v) at the P1 position, categorized into three groups (v_1–v_3) based on their properties (Supplementary Table S31).

Expression, purification, and activation of human pro-cathepsin B

The gene encoding human pro-cathepsin B (Arg18–Ile339) (NP_001899.1) was synthesized by Genewiz, Suzhou, China. This gene was cloned into the pcDNA3.4 vector, which included the IL10 secretory signal peptide and an 8-His tag at the N-terminus. The amino acid sequences are provided below. KOD One™ PCR Master Mix-Blue (ThermoFisher Scientific) was used for PCR amplification of the DNA. The gene fragments

were assembled using the Gibson assembly kit (Vazyme, Cat.# C115-01). The resulting plasmids were transformed into *Escherichia coli* DH5α for amplification. The amplified plasmids were subsequently extracted using a GoldHi EndoFree Plasmid Maxi Kit (CWBio, Cat.# CW2104M). To confirm the enzymatic active site of cathepsin B, a dead mutant (C29A) was constructed based on the wild-type human pro-cathepsin B. Additionally, the S115A mutation was introduced to eliminate primary N-glycosylation[22,40], facilitating the determination of the molecular weight via LC-MS.

Expi293F cells (Invitrogen) were cultured in SMM 293-TII medium (Sino Biological, Lot. RZ14NO1601) at 37 °C under 6% CO_2 in a CRYSTAL shaker (140 rpm). The cells were transiently transfected with plasmids and polyethyleneimine (PEI) (Polysciences, Cat.# 24765-1) when the cell density reached approximately 1.5×10^6/mL. A total of 1.5 mg of plasmid was premixed with 3.9 mg of PEI (1:2.6) in 50 mL of fresh medium for 20 minutes before being added to a 1 L cell culture. The transfected cells were cultured for 84–96 hours before harvesting.

For purification of human pro-CATB, cell supernatants were harvested by centrifugation at 1200× *g* for 5 minutes. Then, the supernatants were loaded onto Ni-NTA beads (Genscript, Cat.# L00666-100) and washed with washing buffer (10–30 mM imidazole, 1× PBS, pH 7.4). The proteins were then eluted with elution buffer (100 mM imidazole, 1× PBS, pH 7.4). Following SDS–PAGE and Coomassie blue staining, the eluents with the highest purity were concentrated to a specific volume and dialyzed into PBS buffer (pH 7.4). The concentrated protein was stored at −80 °C.

The activation buffer is acidic[41], consisting of 25 mM MES, pH 5.5, 1 mM EDTA, and 2 mM DTT. Concentrated proteins were fully activated by dilution at least 50-fold in the activation buffer, followed by incubation at 37 °C for 30 minutes (Supplementary Data S4a, b) or at room temperature for 90 minutes (Supplementary Fig. S3b). Activation efficiency was confirmed by SDS-PAGE and LC-MS. The enzymatic activity of the proteases was assessed using the candidate D-linker (−rkyyG-spacer−) at both high and low [E]/[S] ratios (Supplementary Data S4c).

Expression and purification of antibodies

The pVITRO1-Tz-*CASTi* plasmid was prepared previously[39] and the *CASTi* tag was inserted at the C-terminus of the Tz heavy chain. The anti-Claudin 18.2 antibody plasmids (heavy chain and light chain) were obtained from collaborators (Oricell Therapeutics), and the *CASTi* tag was inserted at the C-terminus of the heavy chain. Expression of the antibody was the same as for the human pro-CATB mentioned above. For the Tz-*CASTi* plasmid, a total of 1.5 mg of plasmid was premixed with 3.9 mg of PEI (1:2.6) in 50 mL of fresh medium. For anti-CLDN18.2-*CASTi*, a 2:1 ratio of light to heavy chain plasmids was prepared, and a total of 1.5 mg of the mixture was premixed with 3.9 mg of PEI (1:2.6) in 50 mL of fresh medium. The medium supernatant was collected by centrifugation at 1,200× *g* for 5 minutes. The supernatants were loaded twice on Protein A beads (GenScript, Cat.# L00210-50) and washed with PBS buffer for 10 column volumes. The antibodies were then eluted with 0.1 M glycine (pH 3.0) and immediately neutralized with 0.2 M $NaHCO_3$ (pH 8.2). The elution was concentrated and subjected to size-exclusion chromatography (Superdex 200 Increase 10/300 GL, GE Healthcare) in N-Methylmorpholine (NMM) buffer (50 mM, 0.2 M NaCl, pH 7.4). Purified proteins were harvested, analyzed by LC-MS, and stored at −80 °C.

Kinetics determination of proteases by LC-MS

The enzyme reaction buffers were identical to those used in the screening, as previously mentioned. The optimal concentration of proteases was measured by pre-experimentation to ensure that 100 μM of substrate could saturate cleavage within 1 hour. For detection experiments, the substrate was diluted in a gradient from millimolar to micromolar concentrations using the reaction buffer and preheated at 37 °C for 5 minutes. The reaction was initiated by adding an equal concentration of protease. The reaction was terminated by sampling and boiling at various time points, and the cleavage was monitored using LC-MS. For the calibration of peak heights, the ratio of peak heights of the target product to those of the raw material was calculated by preparing mixtures of different ratios of the product and raw material, and the ratio corresponding to a low percentage of the product was used as the calibration coefficient. Then, the peak heights of the products and raw materials were calibrated to calculate the actual yields, and the yields were converted to the molar amount of the product based on the substrate concentration. The slope of the linear region of the kinetic assay, obtained from the substrate diluted at gradient concentrations, was selected as the initial reaction velocity (v_0) for fitting the data to the Michaelis-Menten equation.

The k_{cat} and K_m values were obtained by fitting the substrate concentration and initial velocity data to the equation $v_0 = (V_{max}[S])/(K_m + [S])$ using GraphPad Prism software. Here, v_0 represents the initial velocity of the enzyme with its corresponding substrate concentration [S], and V_{max} denotes the maximum enzyme velocity at saturated [S]. $V_{max} = k_{cat}[E]_T$, where $[E]_T$ is the total protease concentration used in the assay. K_m is the substrate concentration [S] at which the reaction rate is half of V_{max}. All data were plotted, calculated, and analyzed using GraphPad Prism 9.5.0.

Co-crystallization and structure determination

Human pro-CATB-S115A was activated in activation buffer (100-fold dilution, 25 mM MES, pH 5.5, 1 mM EDTA, 2 mM DTT) for 90 minutes at room temperature (Supplementary Fig. S3b). Amicon Ultra filter with a 10 kDa cut-off was used to remove DTT and the propeptide. The Ac-rkyyG-hCATB complex was covalently formed by incubating a 5-fold molar excess of Ac-rkyyG-Cl (4 mM in DMSO) with 1.5 mg of active hCATB-S115A in binding buffer (25 mM MES, pH 5.5) for 30 minutes at room temperature[42]. The complex was buffer-exchanged more than four times into binding buffer using an Amicon Ultra filter (10 kDa) and finally concentrated to 10 mg/mL. Ac-YYG-hCATB complex was prepared in the same way as the Ac-rkyyG-hCATB complex (Supplementary Data S3b–d).

The crystallization conditions were screened in 96-well hanging-drop trays from Hampton Research and the temperature was kept at 18 °C. Crystals were grown using the hanging-drop vapor diffusion method by mixing the protein solution and well buffer in ratios of 1:1, 1:2, or 2:1. The Ac-rkyyG-hCATB complex was successfully crystallized in conditions D9 (0.1 M bicine, pH 8.5, 20% w/v PEG 10K, 0.2 μL complex:0.1 μL well-buffer) from the Hampton PEG-Rx HT kit and F10 (0.1 M MES monohydrate, pH 6.5, 12% w/v PEG 20K, 0.1 μL complex:0.2 μL well-buffer) from the Hampton

Crystal Screen HT kit. For sample preparation, crystals were mounted on loops and submerged in a cryoprotectant (reservoir solution plus 20% (v/v) glycerol). Diffraction data were collected using a single-crystal X-ray diffractometer (Rigaku, XtaLAB Synergy Customer) at 100 K. The structure from condition D9 was determined by data reduction and molecular replacement with Phaser in CCP4i2, using PDB 6AY2[26,43] with the ligand removed as the model. The structures were refined iteratively in Phenix. The diffraction data and refinement statistics for Ac-rkyyG-hCATB (PDB: 9XHR) are presented in Supplementary Table S25.

The Ac-YYG-hCATB complex was successfully crystallized in conditions B4 (0.1 M HEPES sodium pH 7.5, 1.5 M lithium sulfate monohydrate, 0.5 µL complex:0.5 µL well-buffer) from the Hampton Crystal Screen HT kit, and F11 (1.6 M ammonium sulfate, 0.1 M MES monohydrate pH 6.5, 10% v/v 1,4-dioxane, 0.15 µL complex:0.1 µL well-buffer) from the Hampton Crystal Screen HT kit. Finally, the structure from condition F11 was analyzed, and the diffraction data and refinement statistics for Ac-YYG-hCATB (PDB: 9VA8) are presented in Supplementary Table S26.

ADC preparation and cytotoxicity assay

Consistent with the published conjugation method[39], a boronic acid reagent with an azide group was synthesized and the *CASTi* tag attached to the C-terminus of the antibody heavy chain was specifically modified. DBCO-PEG3-rkyyG-MMAE and DBCO-PEG3-VC-MMAE (10 mM stock solution in DMSO, 10 equivalents) were added to initiate the click reaction with the azide in PBS buffer (pH 7.4). The mixture was incubated at 37 °C for 2 hours or longer, and the reaction progress was monitored using LC-MS. Upon completion of the reaction, excess peptides were removed by dialysis in PBS. The ADCs were then concentrated, filtered, and quantified using a BCA kit (Beyotime, P0010).

For anti-HER2 ADCs, SK-BR-3 (ATCC HTB-30), JIMT-1 (Procell, CL-0770), and MCF-7 (ATCC HTB-2) were prepared for cell assay, adhering to ATCC guidelines for culture media and conditions. For anti-CLDN18.2 ADCs, AsPC-1-CLDN18.2 and NUGC-4 were prepared for cell assays, with CHO-K1 cells serving as a specificity control. CHO-K1 cells were cultured in Ham's F-12K basal medium, while AsPC-1-CLDN18.2 and NUGC-4, obtained from collaborators (Oricell Therapeutics), were maintained in RPMI-1640 basal medium supplemented with 10% fetal bovine serum (FBS, F8318-500ML), 100 mg/mL streptomycin, and 100 U/mL penicillin. All cells were cultured at 37 °C in a 5% CO_2 environment.

Cells were seeded in a 96-well plate (Corning, Cat.# 3599) at a density of 5×10^3 cells per well (2,500 cells per well for CHO). After a 24-hour incubation, cells were treated with serial dilutions of ADCs, DBCO-MMAE, and antibody-*CAST* for 96 hours, with three replicate wells for each sample. Cell viability was assessed using the Cell Counting Kit-8 (Lablead, Cat.# CK001) according to the manufacturer's protocol and normalized to the viability of untreated cells. Data were plotted and analyzed using GraphPad Prism 9.5.0, employing a nonlinear regression analysis with an inhibitor versus normalized response-variable slope model.

In vitro human, rat, and mouse plasma stability

ICR/CD-1 mouse plasma (IPHASE, Cat.# 0191E1.11), Sprague-Dawley rat plasma (IPHASE, Cat.# 0191D1.11), and human plasma (IPHASE, CAT.# A01911.11) were purchased from IPHASE and were frozen and thawed no more than five times.

For peptide stability, 2 µL of peptides (10 mM stock in DMSO) were individually incubated with 198 µL of plasma at 37 °C. At set time points, 10 µL of samples were taken, and acetonitrile (75% final concentration) was added to precipitate the plasma proteins. The precipitates were removed by centrifugation at 12,000× *g* for 5 min, and the supernatant was diluted 200-fold with solvent A1 and analyzed by Agilent 1260-6230 TOF LC-MS. The amount of peptide remaining was calculated and compared.

For ADCs' stability, 1.2 µL of ADCs (100 µg/mL stock in PBS) were individually incubated with 118.8 µL of plasma at 37 °C. At set time points, 15 µL of the samples were taken and stored at −80 °C for sandwich ELISA analysis.

In vivo mouse pharmacokinetics

Male BALB/c mice (8 weeks old) were purchased from Shanghai Jihui Laboratory Animal Care Co., Ltd., and bred at the Laboratory Animal Resources Center of Westlake University. The mice were acclimated to the animal facility for 1 week following quarantine and were housed under specific pathogen-free conditions. All animal maintenance and experimental procedures adhered to the guidelines of the Institutional Animal Care and Use Committee (IACUC) of Westlake University (Hangzhou, China).

Mice were randomly divided into control and experimental groups ($n = 6$ per group). ADCs were administered intravenously at a dose of 1 mg/kg (100 µL). Blood samples were collected by tail bleeding either before or at specified time points post-injection. The collected blood samples, in heparin-coated tubes, were centrifuged at 1,500× *g* for 10 minutes to isolate the plasma. A protease inhibitor cocktail (Abcam, CAT.# ab271306) and 5 mM EDTA were immediately added to the plasma, which was then stored at −80 °C for subsequent sandwich ELISA analysis. The half-life and area under the curve were determined using PKsolver.

Sandwich ELISA

A high-binding 96-well ELISA plate (Biofil, 190731-080) was coated with in-house-prepared HER2 protein (100 ng per well) diluted in ELISA coating buffer (0.05 M $NaHCO_3$, pH 9.6) overnight at 4 °C. After washing with TBS-T (0.05% Tween 20, pH 7.4), each well was blocked with 5% nonfat dried milk (Beyotime, CAT.# P0216) in TBS-T for 2 hours at room temperature. The wells were then washed again and loaded with diluted proteins or blood plasma samples, followed by incubation at 4 °C overnight. For Tz detection, 100 µL of rabbit anti-human IgG H&L (HRP) (ab6759) (1:5,000) was added to each well at room temperature for 2 hours. For MMAE payload detection, 100 µL of monoclonal anti-MMAE antibody, mouse IgG (Acro, Cat.# MME-M5252) (1:5,000) was added to each well at room temperature for 2 hours, followed by adding 100 µL of HRP-labeled goat anti-mouse IgG(H + L) (Beyotime, A0216) (1:5,000) as a secondary detection antibody. Between all the steps, the plate was washed by filling the wells with 200 µL of TBS-T four times. Finally, 100 µL of TMB (Solarbio Life Sciences) was added to each well and incubated for 10–15 minutes, followed by the addition of an equal volume of 2 M HCl to stop the reaction. The optical density was read at 450 nm with a microplate reader (Varioskan LUX). The data were analyzed using GraphPad Prism V9.5.0, and standard

curves were plotted using PBS diluted protein samples. All data were analyzed by Graphpad Prism 9.5.0.

In vivo antitumor activity

Female NSG mice (four-week old) from the Laboratory Animal Resources Center of Westlake University were used for *in vivo* assay. The mice were adapted to the animal facility for 1 week after quarantine and housed under specific pathogen-free conditions. All animal maintenance and experimental procedures were conducted in accordance with the Institutional Animal Care and Use Committee (IACUC) guidelines of Westlake University (Hangzhou, China).

Subcutaneous xenograft of NUGC-4 tumors with medium expression of the CLDN18.2 receptor was used to evaluate the *in vivo* antitumor activity of the conjugates. The tumor model was constructed by subcutaneous inoculation of 5×10^6 NUGC-4 cells per mouse in 100 µL of RPIM-1640 into the right flanks of the NSG mice. When tumor volumes reached approximately 150 mm^3, the mice were randomly divided into groups ($n = 6$). For treatment, the mice were injected with 12 mg/kg ADC(rkyyG-MMAE), ADC(VC-MMAE), or anti-CLDN18.2 antibody-CAST via the tail vein once a week for a total of four doses. In the control group, the mice were given PBS at the same time points. Tumor growth was measured with a digital caliper, and tumor volumes were calculated using the following formula: $0.52 \times \text{length} \times \text{width}^2$. The body weights of the animals were recorded throughout the experiment. The animals were euthanized when the tumor volume reached 2,000 mm^3. Statistical differences between treatment groups at specific time points were performed using an unpaired two-tailed *t*-test. Differences between groups were considered statistically significant at $P < 0.05$. All statistics were analyzed with GraphPad Prism 9.5.

Molecular modeling and simulation

The computational modeling of enzyme-peptide substrate complexes began with Boltz-2 predictions. In particular, for native L-peptide systems, complex structures were predicted using Boltz-2[44–46], incorporating prior knowledge of the enzyme active site and the substrate cleavage site. Distance restraints between the catalytic residues and the cleavage site were applied during structure prediction to generate multiple initial binding poses. For the mirror-image D-peptide systems, the D-peptides were first constructed using CHARMM[47] and then aligned to the corresponding L-peptide binding pose to generate the mirro-image complex. For each system, multiple initial configurations were generated using different alignment references, and independent MD simulations were used to assess the binding stability and discard unphysical enzyme-substrate complexes.

For MD simulations, all systems were solvated in a cubic box of TIP3P water molecules and neutralized with 150 mM NaCl. Each system was first subjected to energy minimization for 5,000 steps to eliminate steric clashes and then gradually equilibrated through four stages using OpenMM[48]. An initial 200 ps canonical (NVT) ensemble simulation at 298 K with a 1 fs time step was performed, followed by 1 ns NVT equilibration at 298 K with a 2 fs time step; in both stages, protein and peptide backbone atoms were restrained with harmonic potentials of 10 kcal mol^{-1} $Å^{-2}$ and 5 kcal mol^{-1} $Å^{-2}$, respectively. The systems were then equilibrated for 2 ns in the NPT ensemble at 298 K and 1 bar using a Monte Carlo barostat, with restraint force constants reduced to 2 kcal mol^{-1} $Å^{-2}$. Finally, 10 ns isothermal-isobaric (NPT) equilibration without positional restraints was performed. The CHARMM36m force field was used[49]. Long-range non-bonded interactions were fully accounted for, with electrostatics treated with the Particle Mesh Ewald (PME) method and van der Waals interactions using the LJ-PME method with a grid tolerance of 0.0005[50]. Production MD simulations were performed for 200 ns in the NPT ensemble at 298 K and 1 bar, with frames saved every 2 ps. The last 100 ns were used for analysis. Representative bound structures were selected as the medoid of the most populated cluster using K-medoids clustering of the peptide conformations after global alignment of the enzyme-peptide complexes.

DATA AVAILABILITY

The authors declare that all the data supporting the findings of this study are available within the paper, its supplementary information file, or from the corresponding author.

ACKNOWLEDGMENTS

We thank the Mass Spectrometry & Metabolomics Core Facility, the Protein Characterization and Crystallography Facility, the Laboratory Animal Resource Center at the Center for Biomedical Research Core Facilities at Westlake University, and the Instrumentation and Service Center for Molecular Sciences of Westlake University for sample analysis. This work was supported by the Natural Science Foundation of China (32120103013), the "Pioneer" and "Leading Goose" R&D Program of Zhejiang (No. 2024SDXHDX0002, 2025SDXHDX0002), the National Key Research and Development Program of China (2024YFC3407400), Major Program of the National Natural Science Foundation of China (T2596081), Westlake Laboratory of Life Sciences and Biomedicine, the Research Center for Industries of the Future (RCIF) at Westlake University, and Westlake Education Foundation.

AUTHOR CONTRIBUTIONS

B.D. designed the project. M.L. performed the peptide selection, substrate optimizations, cell assays and animal studies. M.L. and T.L. determined the crystal structure. K.C. and M.G. helped with ADC preparations. J.Han helped with peptide synthesis. J.Huang and W.Z. performed MD simulations. J.Z. and X.Z. helped with phylogenetic analysis. B.D., T.L., and M.L. analyzed the data, wrote, and revised the manuscript.

COMPETING INTERESTS

B.D. and M.L. are the inventors of a provisional patent filed by Westlake University. The other authors declare no competing interests.

REFERENCES

1. Siegel, J.S. Homochiral imperative of molecular evolution. *Chirality* **10**, 24–27 (1998).
2. Blackmond, D.G. The origin of biological homochirality. *Cold Spring Harb. Perspect. Biol.* **2**, a002147 (2010).
3. Milton, R.C., Milton, S.C. & Kent, S.B. Total chemical synthesis of a D-enzyme: the enantiomers of HIV-1 protease show demonstrations of reciprocal chiral substrate specificity. *Science* **256**, 1445–1448 (1992).
4. Mandal, K. et al. Chemical synthesis and X-ray structure of a heterochiral D-protein antagonist plus vascular endothelial growth factor protein complex by racemic crystallography. *Proc. Natl. Acad. Sci. USA* **109**, 14779–14784 (2012).

5. Harrison, K. et al. Synthesis and applications of mirror-image proteins. *Nat. Rev. Chem.* **7**, 383–404 (2023).
6. Miller, S.M. et al. Comparison of the proteolytic susceptibilities of homologous L-amino acid, D-amino acid, and N-substituted glycine peptide and peptoid oligomers. *Drug Dev. Res.* **35**, 20–32 (1995).
7. Poreba, M. et al. Fluorescent probes towards selective cathepsin B detection and visualization in cancer cells and patient samples. *Chem. Sci.* **10**, 8461–8477 (2019).
8. Janiszewski, T. et al. Investigation of osteoclast cathepsin K activity in osteoclastogenesis and bone loss using a set of chemical reagents. *Cell Chem. Biol.* **30**, 159–174 (2023).
9. Poreba, M. et al. Selective imaging of cathepsin L in breast cancer by fluorescent activity-based probes. *Chem. Sci.* **9**, 2113–2129 (2018).
10. Schumacher, T.N. et al. Identification of D-Peptide Ligands Through Mirror-Image Phage display. *Science* **271**, 1854–1857 (1996).
11. Qi, Y., Zheng, J. & Liu, L. Mirror-image protein and peptide drug discovery through mirror-image phage display. *Chem* **10**, 2390–2407 (2024).
12. Uppalapati, M. et al. A potent D-protein antagonist of VEGF-A is nonimmunogenic, metabolically stable, and longer-circulating *in vivo*. *ACS Chem. Biol.* **11**, 1058–1065 (2016).
13. Sun, K. et al. Accurate *de novo* design of heterochiral protein-protein interactions. *Cell Res.* **34**, 846–858 (2024).
14. Chorev, M. & Goodman, M. Recent developments in retro peptides and proteins—an ongoing topochemical exploration. *Trends Biotechnol.* **13**, 438–445 (1995).
15. Chorev, M. & Goodman, M. A Dozen years of retro-inverso peptidomimetics. *Acc. Chem. Res.* **26**, 266–273 (1993).
16. Adamala, K.P. et al. Confronting risks of mirror life. *Science* **386**, 1351–1353 (2024).
17. Houghten, R.A. et al. Generation and use of synthetic peptide combinatorial libraries for basic research and drug discovery. *Nature* **354**, 84–86 (1991).
18. Backes, B.J. et al. Synthesis of positional-scanning libraries of fluorogenic peptide substrates to define the extended substrate specificity of plasmin and thrombin. *Nat. Biotechnol.* **18**, 187–193 (2000).
19. Schechter, I. & Berger, A. On the size of the active site in proteases. I. Papain. *Biochem. Biophys. Res. Commun.* **27**, 157–162 (1967).
20. Raran-Kurussi, S. et al. Differential temperature dependence of tobacco etch virus and rhinovirus 3C proteases. *Anal. Biochem.* **436**, 142–144 (2013).
21. Bianchini, E.P. et al. Mapping of the catalytic groove preferences of factor Xa reveals an inadequate selectivity for its macromolecule substrates. *J. Biol. Chem.* **277**, 20527–20534 (2002).
22. Redzynia, I. et al. Displacement of the occluding loop by the parasite protein, chagasin, results in efficient inhibition of human cathepsin B. *J. Biol. Chem.* **283**, 22815–22825 (2008).
23. Kuhelj, R., Dolinar, M., Pungercar, J. & Turk, V. The preparation of catalytically active human cathepsin B from its precursor expressed in Escherichia coli in the form of inclusion bodies. *Eur. J. Biochem.* **229**, 533–539 (1995).
24. Egorova, V.S. et al. Smart Delivery systems responsive to cathepsin B activity for cancer treatment. *Pharmaceutics* **15**, 1848 (2023).
25. Yadati, T., Houben, T., Bitorina, A. & Shiri-Sverdlov, R. The ins and outs of cathepsins: physiological function and role in disease management. *Cells* **9**, 1679 (2020).
26. Wei, B. et al. Discovery of peptidomimetic antibody-drug conjugate linkers with enhanced protease specificity. *J. Med. Chem.* **61**, 989–1000 (2018).
27. Balamkundu, S. & Liu, C.F. Lysosomal-cleavable peptide linkers in antibody-drug conjugates. *Biomedicines* **11**, 3080 (2023).
28. Dorywalska, M. et al. Molecular basis of valine-citrulline-PABC linker instability in site-specific ADCs and its mitigation by linker design. *Mol. Cancer Ther.* **15**, 958–970 (2016).
29. Ubink, R. et al. Unraveling the interaction between carboxylesterase 1c and the antibody-drug conjugate SYD985: Improved translational PK/PD by using Ces1c knockout mice. *Mol. Cancer Ther.* **17**, 2389–2398 (2018).
30. Caculitan, N.G. et al. Cathepsin B is Dispensable for Cellular Processing of Cathepsin B-Cleavable Antibody-Drug Conjugates. *Cancer Res.* **77**, 7027–7037 (2017).
31. Wu, Z., Wright, G.D. & Walsh, C.T. Overexpression, purification, and characterization of VanX, a D-, D-dipeptidase which is essential for vancomycin resistance in Enterococcus faecium BM4147. *Biochemistry* **34**, 2455–2463 (1995).
32. Asano, Y., Ito, H., Dairi, T. & Kato, Y. An alkaline D-stereospecific endopeptidase with beta-lactamase activity from Bacillus cereus. *J. Biol. Chem.* **271**, 30256–30262 (1996).
33. Grandchamps, J. et al. Streptomyces K15 active-site serine DD-transpeptidase: specificity profile for peptide, thiol ester and ester carbonyl donors and pathways of the transfer reactions. *Biochem. J.* **307**, 335–339 (1995).
34. Pratt, R.F., Substrate specificity of bacterial DD-peptidases (penicillin-binding proteins). *Cell. Mol. Life Sci.* **65**, 2138–2155 (2008).
35. Weinstock, M.T., Jacobsen, M.T. & Kay, M.S. Synthesis and folding of a mirror-image enzyme reveals ambidextrous chaperone activity. *Proc. Natl. Acad. Sci. USA* **111**, 11679–11684 (2014).
36. Newcombe, E.A. et al. Stereochemistry in the disorder-order continuum of protein interactions. *Nature* **636**, 762–768 (2024).
37. Choe, Y., Leonetti, F., Greenbaum, D.C., Lecaille, F. & Bogyo, M. Substrate profiling of cysteine proteases using a combinatorial peptide library identifies functionally unique specificities. *J. Biol. Chem.* **281**, 12824–12832 (2006).
38. Dooley, C.T. & Houghten, R.A. Synthesis and screening of positional scanning combinatorial libraries. *Methods Mol. Biol.* **87**, 13–24 (1998).
39. Guo, M. et al. Copper assisted sequence-specific chemical protein conjugation at a single backbone amide. *Nat. Commun.* **14**, 8063 (2023).
40. Mach, L. et al. Proteolytic processing and glycosylation of cathepsin B. The role of the primary structure of the latent precursor and of the carbohydrate moiety for cell-type-specific molecular forms of the enzyme. *Biochem. J.* **282**, 577–582 (1992).
41. Mach, L. et al. Activation of pro-cathepsin B in human hepatoma cells: the conversion into the mature enzyme relies on the action of cathepsin B itself. *Biochem. J.* **293**, 437–442 (1993).
42. Greenspan, P.D. et al. Identification of dipeptidyl nitriles as potent and selective inhibitors of cathepsin B through structure-based drug design. *J. Med. Chem.* **44**, 4524–4534 (2001).
43. Schmitz, J. et al. Cathepsin B: Active site mapping with peptidic substrates and inhibitors. *Bioorg. Med. Chem.* **27**, 1–15 (2019).
44. Passaro, S. et al. Boltz-2: Towards accurate and efficient binding affinity prediction. *bioRxiv* 2025.06.14.659707 (2025).
45. Wohlwend, J. et al. Boltz-1 democratizing biomolecular interaction modeling. *bioRxiv* 2024.11.19.624167 (2025).
46. Mirdita, M. et al. ColabFold: Making protein folding accessible to all. *Nat. Methods* **19**, 679–682 (2022).
47. Brooks, B.R. et al. CHARMM: the biomolecular simulation program. *J. Comput. Chem.* **30**, 1545–1614 (2009).
48. Eastman, P. et al. OpenMM7: Rapid development of high performance algorithms for molecular dynamics. *PLoS Comput. Biol.* **13**, e1005659 (2017).
49. Huang, J., Rauscher, S., Nawrocki, G., Ran, T., Feig, M. & de Groot, B.L. CHARMM36m: an improved force field for folded and intrinsically disordered proteins. *Nat. Methods* **14**, 71–73 (2017).
50. Xu, Y. & Huang, J. Validating the CHARMM36m protein force field with LJ-PME reveals altered hydrogen bonding dynamics under elevated pressures. *Commun. Chem.* **4**, 99 (2021).

ADDITIONAL INFORMATION

Supplementary information The online version contains supplementary material available at https://doi.org/10.15302/vita.2026.03.0022.

Correspondence and requests for materials should be addressed to Jing Huang, Tian Li, or Bobo Dang.